The biochemical mechanisms of antimicrobial photodynamic therapy

Sabino, C.P.[1,2]; Ribeiro, M.S.[3]; Wainwright, M.[4]; dos Anjos, C.[5,6,7]; Sellera, F.P.[5,8]; Dropa, M.[9]; Nunes, N.B.[10]; Brancini, G.T.P.[10]; Braga, G.U.L.[10]; Arana-Chavez, V.E.[11]; Freitas, R.O.[12]; Lincopan, N.[2,13]; Baptista, M.S.[14]

[1]BioLambda, Scientific and Commercial Ltd., São Paulo, SP, Brazil, 05595-000

[2]Department of Clinical and Toxicological Analysis, School of Pharmaceutical Sciences, University of São Paulo, São Paulo, SP, Brazil, 05508-000

[3]Center for Lasers and Applications, Energy and Nuclear Research Institute, São Paulo, SP, Brazil, 05508-000

[4]School of Pharmacy & Biomolecular Sciences, Liverpool John Moores University, Liverpool, UK

[5]Department of Internal Medicine, School of Veterinary Medicine and Animal Science, University of São Paulo, São Paulo, SP, Brazil, 05508-270

[6]Wellman Center for Photomedicine, Massachusetts General Hospital, Harvard Medical School, Boston, Massachusetts, USA

[7]Vaccine and Immunotherapy Center, Massachusetts General Hospital, Harvard Medical School, Boston, USA.

[8]School of Veterinary Medicine, Metropolitan University of Santos, Santos, SP, Brazil, 11080-300.

[9]Public Health Laboratory, School of Public Health, Universidade de São Paulo, São Paulo, Brazil

[10]Faculdade de Ciências Farmacêuticas de Ribeirão Preto, Universidade de São Paulo, Ribeirão Preto, SP, 14040-903, Brazil

[11]Department of Biomaterials and Oral Biology, University of São Paulo, São Paulo, São Paulo, Brazil

[12]Brazilian Synchrotron Light Laboratory, Brazilian Center for Research in Energy and Materials, 13083-970, Campinas, SP, Brazil, 13083-970

[13]Department of Microbiology, Institute for Biomedical Sciences, University of São Paulo, São Paulo, SP, Brazil, 05508-000

[14]Department of Biochemistry, Institute of Chemistry, University of São Paulo, São Paulo, SP, Brazil, 05513-970

Highlights

- *Klebsiella pneumonia* strains with different drug resistance profiles show the same methylene-blue induced phototoxicity.
- Membrane and DNA damage represent contributing factors to bacterial inactivation by aPDT, but are not correlated with the threshold of cell death.
- Protein damage is best correlated with the primary *causa mortis* of *Klebsiella pneumonia* cells.
- aPDT can effectively inactivate drug-resistant microorganisms and simultaneously block drug resistance transmission and dissemination.

Abstract

The unbridled dissemination of multidrug-resistant pathogens is a major threat to global health and urgently demands novel therapeutic alternatives. Following the current trend, the WHO expects that therapeutic options will run out by 2050. Antimicrobial photodynamic therapy (aPDT) has been developed as a promising approach to treat localized infections regardless of drug resistance profile or taxonomy. Even though this technique has been known for more than a century, discussions and speculations regarding the biochemical mechanisms of microbial inactivation have never reached a consensus on what is the primary cause of cell death. Since photochemically generated oxidants promote ubiquitous reactions towards several biomolecules, researchers simply assumed that all cellular structures are equally damaged. In this study, biochemical, molecular biology, and advanced microscopy techniques were employed to investigate if protein, membrane, or DNA damage correlates better with dose-dependent microbial inactivation kinetics. Herein, we showed that although mild membrane permeabilization and late DNA damage occurs, no correlation with inactivation kinetics was found. On the other hand, protein degradation was analyzed by 3 different methods and showed a dose-dependent trend that matches microbial inactivation kinetics. Our results provide a deeper mechanistic understanding of aPDT that can guide the scientific community towards the development of optimized photosensitizing drugs and also rationally propose synergistic combinations with antimicrobial chemotherapy.

Introduction

The catastrophic emergence of microbial drug resistance is a global health priority (1). This scenario is likely to worsen following the COVID-19 pandemic crisis since antibiotics have been widely used to treat bacterial co-infections and/or secondary infections. The major concern on drug resistance dissemination relies on the rapid bacterial ability to acquire resistance genes from prior generations as well as from other strains and species (2-6). A post-antibiotic era could mean the end of current ideas of modern medicine due to the consequent inability to treat common minor infections or to support other areas such as transplants and oncology.

Antimicrobial photodynamic therapy (aPDT) has been successfully used for over a century in modern medicine to treat superficial infections (7, 8). It is an elegant method to produce many strong oxidant substances (*e.g.*, excited-state species and free-radicals) in a space-time-controlled manner that is triggered by light. Such a mechanism of action can simultaneously damage several vital molecules and structures (*e.g.*, proteins, nucleic acids, and membranes) leaving a questionable hypothesis on whether microbes could ever develop a resistance mechanism. On the other hand, aPDT has the broadest action-spectrum possible, as it can neutralize any type of pathogen, such as bacteria, fungi, algae, protozoa, viral particles, and prions (9-12). Currently, the convergence of two independent phenomena has provided an exponential interest in aPDT: the outbreak of drug-resistant microbes demanding alternative therapeutic strategies and the photonic revolution that allow the development of new cost-effective antimicrobial technologies that are not sensitive to the selection of resistant strains.

Despite the great potential of aPDT, the currently used photoactivated drugs, generally referred to as photosensitizers (PSs), are the same as those developed decades or even more than a century ago. Yet, mechanistic understanding of cell killing remains unsophisticated. Current hypotheses only regard the direct action of reactive oxygen species produced by the two established types of photodynamic reactions: electron-transfer (type I) and energy transfer (type II) (13). It is also established that cellular uptake of positively-charged (cationic) PS benefit from electrostatic interactions with negatively-charged (anionic) surface moieties of Gram-negative, Gram-positive bacteria and fungi, whereas repulsion may occur with anionic PS. More detailed mechanistic information is necessary to rationally develop optimized PSs for antimicrobial applications so that synergistic applications may be

developed with classic antimicrobial chemotherapeutics, *i.e*., if a PS is optimized for protein damage, this could be combined with a cell wall-targeting chemotherapeutic antimicrobial.

Although the strong oxidants generated during aPDT can damage various vital cellular components, the sites of critical damage responsible for microbial inactivation have not been established. Thus, major damage at membranes (14), proteins (15, 16), or nucleic acids (17) has never been specifically linked to cell death.

In this article we report an experimental protocol that allows deeper insights into the biochemical mechanisms of aPDT. For our experiments, we used carbapenem-resistant *K. pneumoniae* strains because they are ubiquitous pathogens classified as critical global priority by the WHO and present a relatively complex cellular structure as it is a Gram-negative capsulated bacterium. Methylene blue (MB) was employed as a model photosensitizing drug because it undergoes through both types of photodynamic reactions and it is also the most popular and broadly available photosensitizer used for aPDT. Taken together, our results demonstrate that proteins play a pivotal role in microbial killing since protein degradation matches microbial inactivation kinetic promoted by aPDT.

Results

To match the maximum absorption peak of MB monomers at 664 nm, we developed a customized LED system with peak emission at 662(21) nm. The spectral characteristics of LED and MB are plotted in **Figure 1a**. Using equation 2, the number of absorbed photons was calculated as a function of wavelength (**Fig. 1b**). Results indicate that 64.6 % of incident light was absorbed by our MB solution at the same parameters used in aPDT assays, resulting in the absorption of 2.62×10^{22} photons per second. According to the molarity of the experimental solution, it is estimated that, on average, each MB molecule is being excited 4.3×10^{5} times per second. Since the singlet oxygen yield of MB has an average efficiency of 50 %, each molecule would be able to produce up to 2.1×10^{5} singlet oxygen molecules per second. No microbial cell is expected to tolerate such an oxidative insult for long or to be able to develop an effective resistance mechanism to such approach.

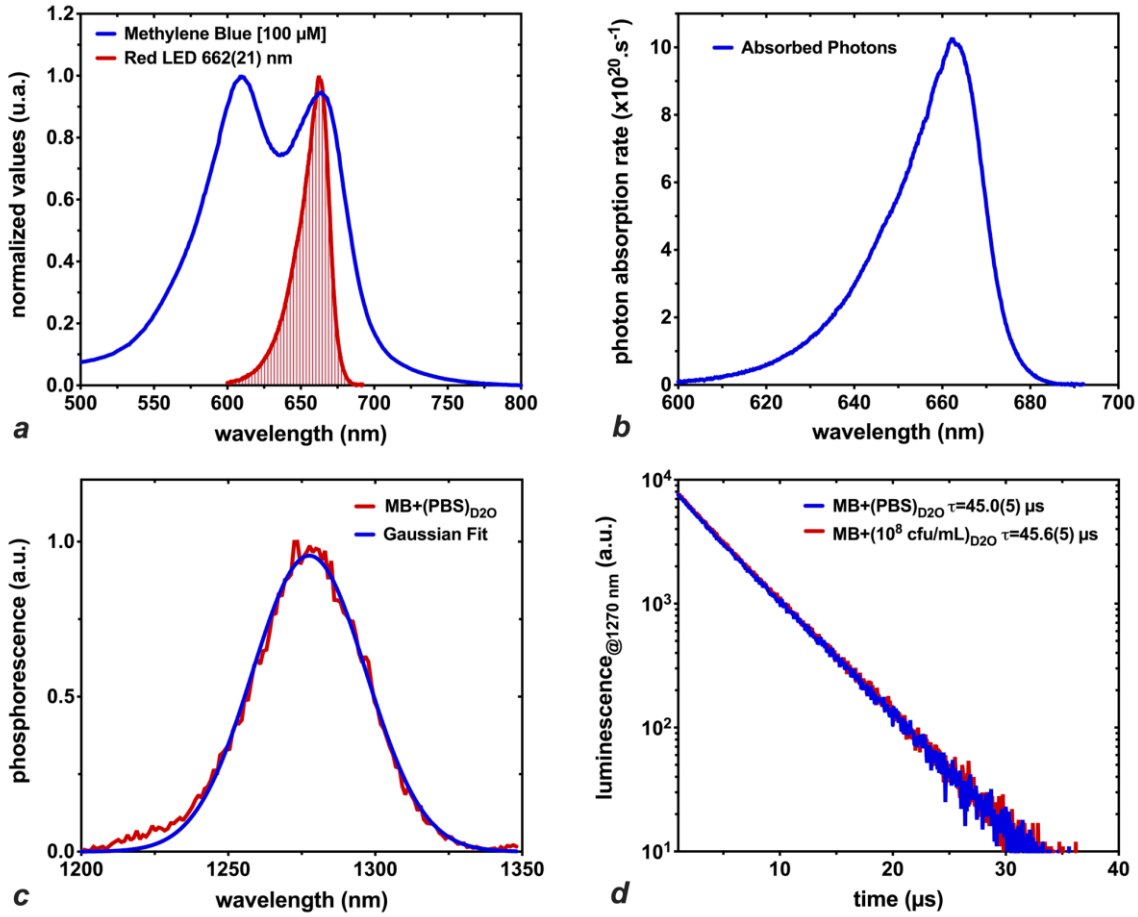

Figure 1. ***a*)** Spectral emission of LED system and absorption of MB; ***b*)** Spectrum resolved light absorption of the irradiation system used in this work; ***c)*** Phosphorescence spectrum of singlet oxygen in PBS solution prepared with D_2O with or without bacterial inoculum presented peak emission at 1277 nm; ***d*)** Lifetime around 45 µs.

The characteristic singlet oxygen phosphorescence peak was observed around 1277 nm and its normality was confirmed by Gaussian fit (**Fig. 1c**). According to exponential fit parameters, phosphorescence lifetime fluctuated around 45 µs and the addition of 10^8 CFU/mL was not enough to quench the phosphorescence in detectable levels when measurements were performed in solution (**Fig. 1d**). The fact that singlet oxygen can be generated within bacterial cells indicates that not only that it may be involved itself in the cell-killing but, perhaps more importantly, that triplets are generated in abundant levels close to the molecular targets, being therefore prone to initiate contact-dependent reactions with relevant biomolecules, such as proteins, nucleic acids, carbohydrates and membranes constituents.

Inactivation kinetics curves of all three *Klebsiella pneumoniae* strains tested in this study are presented in **Figure 2a.** Lethal doses for 90% inactivation were 4.3 ±0.3 J/cm^2 for ATCC 700603, 4.7 ± 0.4 J/cm^2 for ATCC BAA1705 and 6.4 ±0.6 J/cm^2 for BR-1 with statistically significant differences between BR-1 and ATCC 700603 or ATCC BAA1705. The tolerance factor (T) was 0.81 ± 0.04 for ATCC 700603, 0.93 ± 0.07 for ATCC BAA1705, and 1.1 ± 0.1 for BR-1 only with statistically significant differences between BR-1 and ATCC 700603. Even though some statistically significant differences were found, it is noticeable that inactivation kinetics rates were very similar amongst all strains.

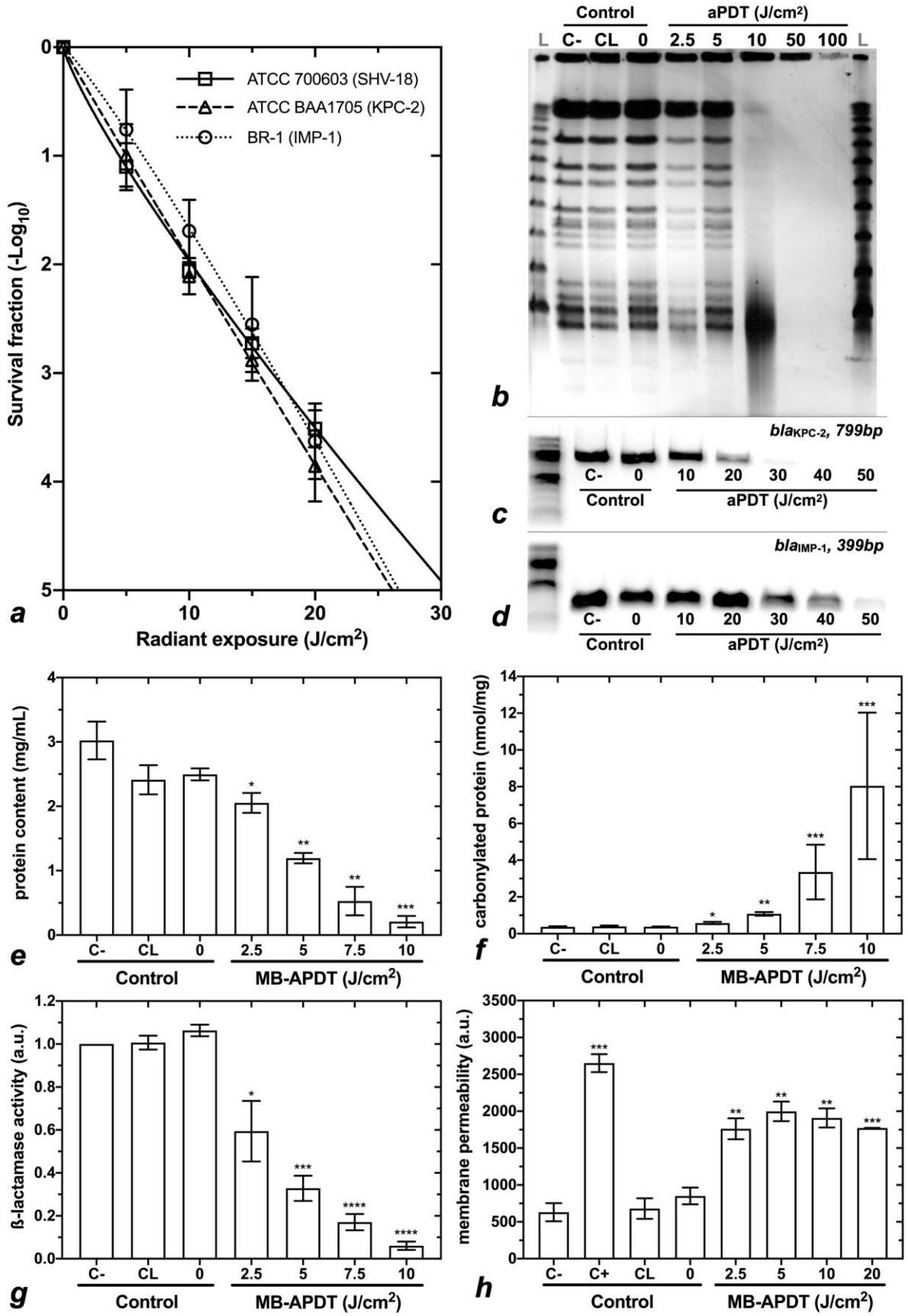

Figure 2. ***a*)** Inactivation kinetics of aPDT against *K. pneumoniae* strains. All strains had very similar inactivation kinetics curves and the lethal dose for 90% of inactivation fluctuated around 5 J/cm^2; ***b*)**

Analysis of DNA damage by electrophoresis presenting the PFGE result of the total *K. pneumoniae* DNA. C– refers to negative (sham) controls, CL are controls only treated with 100 J/cm^2 of light, 0 are controls only treated with PS for 1 h and L are molecular weight reference ladders of 5Kb. Double-strand DNA breaks induced by aPDT caused the formation of smaller fragments of random sizes giving the smear impression seen in group 10 J/cm^2. In higher dose groups (*e.g.*, 50 and 100 J/cm^2), such small fragments were formed that no retention is visible in the electrophoresis gel; ***c*** **and** ***d*****)** PCR amplification products of *K. pneumoniae* carbapenemase-encoding genes before and after aPDT. Greyscale fluorescence images allow clear visualization of amplicon size and dose-dependent fading of PCR-amplification bands induced by aPDT; Degradation kinetics of proteins presented as loss of protein content **(*e*)**, carbonylation of proteins **(*f*)**, and inhibition ß-lactamase enzymatic activity (SHV-18, produced by *K. pneumoniae* ATCC 700603) **(*g*)**. Membrane permeability assay **(*h*)** was measured by *N*-phenyl-1-naphthylamine (NPN) uptake. C- are negative (sham) controls, C+ are positive controls for membrane damage treated with propyl alcohol at 70% for 15 min, CL are controls only treated with 20 J/cm^2 of light, 0 are controls only treated with 100 µM of MB for 1 h. It can be noticed that protein degradation continuously increases in a dose-dependent manner while cell permeability is significantly increased at the beginning of the irradiation process (2.5 J/cm^2) but remains unchanged until 20 J/cm^2. Single asterisks (*) represent $p<0.05$, double asterisks (**) represent $p<0.01$, triple asterisks (***) represent $p<0.001$, and quadruple asterisks (****) represent $p<0.0001$ differences compared to the negative control group (C-).

Since MB molecules bind DNA (18), and assuming that in this system each PS molecule might be excited around 4.3x10^5 times per second, it is reasonable to suppose that DNA damage can be expressive. Purine bases are common targets for singlet oxygen and hydroxyl radicals while the ribose-phosphate backbone structure is mostly sensitive to hydroxyl-radicals (19, 20). To elucidate these valuable findings, the DNA damage of chromosomes and plasmids were investigated by pulsed-field gel electrophoresis (PFGE, **Fig. 2b**) and also important drug resistance genes (e.g., *bla*$_{\text{IMP-1}}$ and *bla*$_{\text{KPC-2}}$) by PCR (**Fig. 2c-d**). Considering the singlet oxygen formation rate above-mentioned, it is unlikely that microbial cells can repair the DNA damage at a sufficient rate to resist inactivation.

PFGE analysis of the degradation of chromosomal DNA (**Fig. 2b**) presented a loss of band pattern, forming a smear aspect at 10 J/cm^2. At 50 and 100 J/cm^2, DNA is fragmented in such small sections that they were nearly not retained in the gel matrix. Assuming that single event DNA damage can impair DNA-polymerase or ribosomal activity, the amplification of DNA in genes related to carbapenemase resistance following crescent doses of aPDT was attempted. Dose-dependent inhibition of DNA amplification is observable (**Fig. 2c-d**). The inhibition level was also

dependent on the amplicon sequence size. The more sensitive *bla*$_{KPC-2}$ amplicon is 799bp long and began presenting amplification inhibition at 20 J/cm^2 while *bla*$_{IMP-1}$ is half as long (399bp) and presented the same level of amplification inhibition at 40 J/cm^2. It indicates that damage probability must be directly proportional to the DNA sequence size or – in other words – simply the number of targets. Consequently, hit points for oxidative damage during aPDT must have a greater impact on a target the size of chromosomal DNA. However, comparing these dose-dependent DNA degradation results (**Fig. 2b-d**) to the cellular inactivation kinetics (**Fig. 2a**) it remains questionable whether DNA damage contributes directly to microbial inactivation since the LD_{90} is reached at around only 5 J/cm^2. This suggests that extensive DNA damage only occurs after bacterial cells are already dead.

Insightful results were obtained on protein damage analysis (**Fig. 2e-g**). Significant loss of protein content (**Fig. 2e**) and increase of protein carbonylation (**Fig. 2f**) were observed, which continuously progressed in a dose-dependent manner. The results show a tendency towards significantly higher protein carbonylation already at 2.5 J/cm^2, which continuously increases with no saturation point over the analyzed range. Longer exposures to light (e.g., 7.5 and 10 J/cm^2) lead to such severe protein loss that the precision of carbonyl content quantification was reduced, although protein loss is itself an indicator of extensive protein oxidation (16, 21). Regarding the enzymatic activity of ß-lactamase (**Fig. 2g**), a continuous dose-mediated enzymatic inhibition is presented in a similar trend as the observed for loss of protein content in **Figure 2e** and is inversely proportional to the carbonylation of proteins (**Fig. 2f**). Therefore, measurements of enzymatic activity precisely confirm the effects of protein loss and carbonylation over protein function.

Membrane permeability, on the other hand, rapidly increases and saturates in intermediary levels resulting in no dose-dependent pattern (**Fig. 2h**). All aPDT experimental data presented statistically significant differences compared to both, C– and C+, indicating that mild membrane damage occurs but it is not as intense as that caused by exposure to 70% propyl alcohol.

Analysis via fluorescence-lifetime imaging microscopy (FLIM) indicates that the MB effectively permeates the microbial cells (**Fig. 3a-f)** and interacts with DNA (**Fig. 3b,e**) and other intracellular content that is densely populated by proteins (**Fig. 3a,d**). Fluorescence lifetime for MB molecules embedded in the cytoplasm is 0.6 ns and for molecules interacting with DNA, it becomes 1.8 ns (**Fig. 3a-d and 3b-e**).

Compartmentalized *Candida albicans* cells demonstrate longer MB fluorescence lifetimes in DNA-rich compartments, such as nuclei and mitochondria (**Fig. 3b**). This is also seen inside *K. pneumoniae* cytosol (**Fig. 3e**).

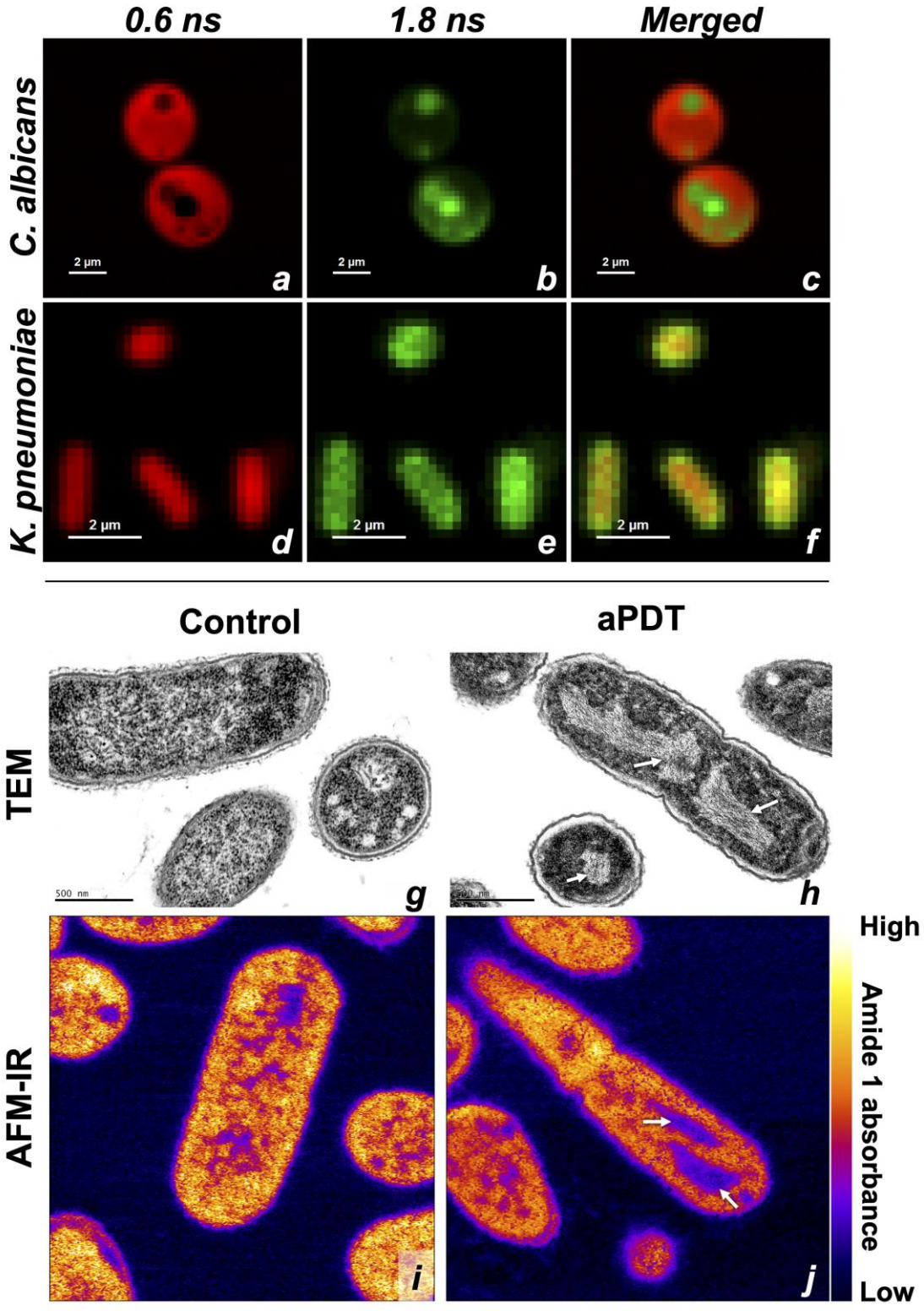

Figure 3. Fluorescence-lifetime imaging microscopy (FLIM) images of MB interacting with *C. albicans* (***a, b, c***) and *K. pneumoniae* (***d, e, f***) cells. Images on ***a*** and ***d*** show the fluorescence signal of

MB interacting with proteins in cytosol presented an average lifetime of 0.6 ns. On ***c*** and ***e***, stabilized MB interacting with DNA presented a three-times higher fluorescence lifetime with an average of 1.8 ns. Images ***c*** and ***f*** show the merged fluorescence signal in each cell type, whereas *C. albicans* organelles facilitate the specificity visualization of this technique. Scale bars represent 2 µm. Nanoscopy images of (***g*** and ***i***) control and (***h*** and ***j***) aPDT-treated cells of *K. pneumoniae* at 100 J/cm^2. Transmission electron microscopy (TEM) images (***g*** and ***h***) were acquired at 80,000x original magnification. Atomic force microscopy coupled to infrared-spectroscopy (AFM-IR) images (***i*** and ***j***) were acquired in contact mode. Observe that aPDT-treated cells tend to aggregate protein content around the intracellular periphery leaving DNA content accumulated in the central region of the cell (indicated by arrows).

Nanoscopy analysis performed by scanning transmission electron microscopy (TEM, **Fig. 3g-h**) and infrared photothermal expansion nanoscopy (AFM-IR, **Fig. 3i-j**) comparing non-treated cells to those exposed to 100 J/cm^2 of aPDT are presented in **Figure 3g-j**. According to **eq. 4**, the dose required to inactivate 100% (*i.e.*, 9 $\log_{10}$) of cells is 64 J/cm^2 for ATCC 700603, 50 J/cm^2 for ATCC BAA1705 and 45 J/cm^2 for BR-1 strains, respectively. Even though cells were treated with a light dose much higher than necessary to inactivate 100% of cells, TEM and AFM-IR images revealed only moderate differences concerning non-treated cells. For this control condition, cellular morphology was noticed to be well preserved, intracellular content well distributed and no sign of cell membrane rupture (**Fig. 3g,i**). However, aPDT-treated cells presented a tendency to aggregate protein content around the intracellular periphery leaving DNA content accumulated in the central region of the cell (indicated by white arrows, **Fig. 3h,j**). Since the AFM-IR laser was tuned to be centered at the amide 1 IR absorption band (1640 cm^{-1}), it is also possible to confirm that such DNA rich areas contain very small quantities of proteins (**Fig. 3j**). TEM images also allow the visualization of DNA strands in the same region **(Fig. 3h)**.

Discussion

Our data is in agreement with a recently published study that compared the inactivation kinetics of multidrug-resistant (MDR) bacteria and yeast concerning their drug-sensitive counterparts (10). Whereas aPDT inactivation kinetics is strongly correlated with microbial species (10), here we show that there is no correlation between photosensitivity and drug resistance profiles of different *Klebsiella pneumoniae* strains.

The formation of carbonyl groups resulting from the photo-oxidation of proteins has been extensively reported and is thought to be a result of side-chain oxidation of susceptible amino acids by reactive oxygen species (15, 16, 23). Therefore, the extent to which photodynamic treatment affected protein carbonyl content was evaluated using a dose-dependent analysis (see **Fig. 2**). Protein loss is another known consequence of photodynamic treatment as oxidative damage to proteins can lead to both aggregation and fragmentation (15, 16). Protein aggregation and cross-linking normally occur after the formation of reactive carbonyl functions on amino acid residues followed by a nucleophilic attack by the sidechains of His, Lys, Arg, and Cys (15, 24, 25). Fragmentation is thought to be a consequence of protein peroxides generated after singlet oxygen reaction with Tyr, His, and Trp residues. The catalyzed decomposition of such peroxides by metals can yield radicals that may propagate the oxidations through chain reactions (26). These can generate α-carbon radicals via hydrogen abstraction which, in turn, results in the formation of Schiff bases involving the amide nitrogen on peptide bonds, ultimately leading to backbone cleavage (27).

Yet, loss of ß-lactamase activity may be a very important factor allowing increased sensitivity to antibiotic therapy of drug-resistant strains that were exposed to sublethal doses of aPDT. In this regard, *K. pneumoniae* strains carrying carbapenemase genes have been under the spotlight of scientific awareness, being classified by the WHO as global critical-priority pathogens (4, 6). The production of extended-spectrum ß-lactamase (ESBL) and carbapenemases - antimicrobial-cleaving enzymes without ATPase activity - are important examples flagging the awareness towards MDR and extensively-drug resistant (XDR) phenotypic profiles. In practical terms, the existence of such phenotypes restrains the use of most commercially-available broad-spectrum bactericidal antibiotic options (28). Therefore, the necessity of novel antimicrobial strategies that are not susceptible to microbial resistance, such as aPDT, is urgent demand.

It is well-known that MB intercalates with DNA double-strands allowing more stable excited states by shielding vibronic interactions with water (18). MB intercalation in GC pairs of the DNA sequence strongly affects its fluorescence lifetime due to Coulomb and van der Waals interactions (19). Intercalation in AT pairs also occurs, but hydrogen bonding is not possible because of the absence of donors inside the minor groove (20, 21). Thus, the MB fluorescence lifetime is longer when intercalated in DNA than when solvated by water or interacting with other biomolecules. This result

brings a prime information on MB distribution and interaction inside yeast and bacterial cells revealed by FLIM photomicrographs.

Membrane damage levels imposed by photodynamic reactions of phenothiazinium compounds have previously been related to the amphiphilicity of the PS molecule. More lipophilic molecules, such as dimethyl methylene blue and DO15, can efficiently induce membrane rupture while the more hydrophilic MB and toluidine blue are not nearly as potent in achieving this effect (14). However, although moderate levels of membrane permeabilization (see **Fig. 2h**) were observed, there were no signs of membrane rupture, even after exposure to aPDT doses much higher than those necessary to induce complete microbial inactivation (see **Fig. 3h,j**). Therefore, membrane and even DNA damage may represent contributing factors to bacterial inactivation by aPDT, although protein damage is the principal cause of cell death.

Antimicrobial chemotherapeutic strategies generally target a unique action site found in specific microbial biomolecules or metabolic pathways to achieve cellular inactivation. This approach facilitates the development or selection of resistant populations as these may be a few mutations away. Most antimicrobials are derivatives of natural fungal or bacterial metabolites that have been used by these microbes to survive in their ecosystems. In this context, some microorganisms have naturally developed intrinsic resistance phenotypes also to thrive in the environment. Hence, genes of naturally occurring drug resistance can already be available via vertical and horizontal transmission, based on the microbial ability to acquire function through the uptake of mobile genetic elements (*e.g.,* transformation, transduction, or conjugation). Membrane rupture may facilitate the horizontal transmission of resistance genes by environmental dissemination of genetic material. Thus, from the current perspective, aPDT works in an ideal mode where inactivated cells keep their damaged DNA and protein content sealed inside the cell.

Even though the cytotoxic effects of aPDT towards bacteria have been known for over a century, no one has ever stated the primary *causa mortis* of bacterial cells. Here, it was observed that the PS effectively permeates microbial cell membranes and even binds with DNA molecules and leads to significant damages to both structures. However, by comparing the dose-dependent degradation of DNA, membrane, and protein structures, it is clear that protein damage best correlates with cell killing. This correlation between irreversible protein damage (as measured by protein carbonylation) and cell death has previously been reported for other types of stress,

such as ultraviolet and ionizing radiation (22). In the extremophilic bacterium *Deinococcus radiodurans*, protein carbonylation was found to be the causal agent of cell death after radiation exposure (23). Indeed, extreme tolerance of *D. radiodurans* to stress is thought to be a consequence of a very efficient antioxidative system protecting the proteome (23, 24). This raises the question of whether aPDT could overcome such efficient proteome protection. However, photoinactivation of *D. radiodurans* was easily achievable (25), further showing that aPDT is very efficient at damaging essential proteins. As an example, photoinactivation of *C. albicans* cells with new methylene blue N at 20 J/cm² resulted in oxidation of 100% of His amino acids and thus no His-containing protein escaped photo-oxidation (26).

Another remarkable interpretation of this mechanism of action is that microbial inactivation can be achieved while damaged and non-functional drug resistance enzymes and genes remain sealed inside the plasma membrane. This fact suggests that aPDT can effectively inactivate drug-resistant microorganisms and simultaneously block drug resistance transmission and dissemination. Consequently, aPDT should become an even more interesting approach shortly as antimicrobial resistance is only expected to increase.

In summary, we unravel the biochemical mechanisms of aPDT. Based on our results, protein damage is the main pathway behind photodynamic microbial inactivation. We hypothesize that protein degradation is the cause for, rather than a consequence of, cell death and that resistance to aPDT would require an entire system of proteome protection that is unlikely to emerge in treated pathogens. The results presented can provide a better mechanistic understanding of aPDT for the development of optimized photosensitizing drugs and also rationally support synergistic combinations with conventional antimicrobial chemotherapeutics.

Materials & Methods

Photosensitizer and light source

Methylene blue (MB, Sigma-Aldrich, USA) as a standard PS, whereby microbial inactivation was calculated based on light radiant exposure (equation 1, J/cm^2) and the number of photons absorbed per volume (equation 2, *AbsorbedPhotons*/cm^3). Stock solutions of MB were prepared in type-1 Milli-Q water, at 10 mM. The MB stock

solutions were filtered by 0.22 µm membrane for decontamination and stored at 4º C in the dark before use.

The LED system (LEDsaber Prototype 1, BioLambda, Brazil) to sample distance was adjusted to achieve a beam-spot diameter of 25 mm, which covered the entire bottom of a well in a 12-well plate. Light irradiance was adjusted to a standard radiant exposure rate (*dR/dt*) of 100 mW/cm^2 (measured at the sample bottom) and beam divergence of 45°. Beam spot on samples was highly homogeneous, with irradiance divergence between center and border below 10%. The LED spectral emission was measured by a UV-VIS spectrophotometer (Flame, Ocean Optics, USA).

Radiant exposure [J/cm^2] is calculated as the product of mean optical power ($\overline{P}$) [mW] and exposure time [s], divided by the beam area [cm^2]. To estimate the number of absorbed photons per volume of solution [V - cm^3], the PS absorption spectrum $A_{(\lambda)}$ and the spectral radiant power emitted by the LED system $P_{(\lambda)}$ were measured. The absorption spectrum of MB was measured in a plate-reader spectrophotometer (SpectraMax M4, Molecular Devices, USA). MB concentration in phosphate-buffered saline (PBS) was 100 µM and the optical path was 2 mm (corresponding to the height of 1 mL solution in a 25 mm cylindric well). Moreover, the universal constant of the velocity of light in vacuum (c_0= 299,792,458 m/s) and the Planck constant (h= 6.62606957×10^{-34} J.s) were used.

$$Radiant\ Exposure = \frac{\bar{P}.t}{Area} \qquad \text{equation (1)}$$

$$\frac{AbsorbedPhotons}{s.cm^3} = \int_{\lambda_0}^{\lambda} \frac{P_{(\lambda)}.10^{A(\lambda)}}{V.c_0.h} d\lambda \qquad \text{equation (2)}$$

The inactivation kinetics analysis method described by Sabino et al. (27) was used as follows in equation 3. Curve fitting and numeric operations were calculated in Prism 7.0 (GraphPad, USA) interface.

$$log_{10}\left(\frac{N_0}{N}\right) = \left(\frac{Dose}{LD_{90}}\right)^T \qquad \text{equation (3)}$$

$$LD_i = LD_{90}\left(-log_{10}\left(1-\frac{i}{100}\right)\right)^{1/T} \qquad \text{equation (4)}$$

where:

N_0= initial microbial burden; N= final microbial burden; *Dose*= radiant exposure (J/cm^2); LD_{90}= lethal dose for 90% of microbial burden (J/cm^2); T= tolerance factor; i= inactivation percentage (%).

aPDT – Sample irradiation studies

K. pneumoniae was used as the bacterial model due to its profound association with extensive drug-resistance. The ATCC 700603 strain *K. pneumoniae* expressing SHV-18 extended-spectrum ß-lactamase (ESBL) was used in all experiments except for polymerase chain reaction (PCR) analysis where KPBr-1 (GenBank accession number: NZ_PDMV00000000.1) and ATCC BAA1705 strains expressing IMP-1 and KPC-2 carbapenemases, respectively, were employed.

Standard aPDT susceptibility test was performed based on Sabino *et al.* (27). Inocula were prepared from log-phase overnight bacterial cultures. Cells were then washed twice in PBS (dibasic phosphate = 2.65 g/L, monobasic phosphate = 0.358 g/L, NaCl = 8.183 g/L and milli-Q water). The turbidity of cell suspensions in PBS was measured in a spectrophotometer to obtain inocula at McFarland scale 4. The scale was calibrated to obtain OD of 0.67 at 625 nm resulting in 1-2 x 10^9 CFU/mL of working concentration of planktonic bacteria.

For bacterial inactivation kinetics assays, aPDT groups were subdivided into 5 groups of variable radiant exposures in steps of 5 J/cm^2. For membrane, protein, and DNA degradation kinetics assays, radiant exposure steps were set according to the detection sensitivity of each method that was predetermined in pilot studies. To avoid cross light exposure, each sample was kept in individual microtubes in the dark during the pre-irradiation time and placed in the 12-wells plate only for irradiation.

For bacterial survival analysis, the simplified method of colony counting established by Jett *et al.* (28) was used. Immediately after irradiation, bacterial suspensions were serially diluted in PBS to give dilutions from 10^{-1} to 10^{-6} times the original concentration. Ten-µL aliquots of each dilution were streaked onto Muller-Hinton agar plates, in triplicates, and incubated at 37° C overnight. The colonies were

counted and converted into normalized $\log_{10}$ units of CFU/mL (colony-forming units per milliliter).

Singlet oxygen detection in solution

Phosphorescence intensity and the lifetime of singlet oxygen ($^1O_2$) produced were measured using a near-infrared (NIR) spectrophotometer. In this assay, the MB solution was prepared in deuterium oxide (D_2O, 99% pure, Sigma-Aldrich), to optimize $^1O_2$ phosphorescence signal (peak emission $\cong$ 1270 nm). MB solutions [100 µM] were prepared either alone or in the presence of 10^8 CFU/mL of *K. pneumoniae*.

MB excitation was pumped by a Nd:YAG tunable laser (λ = 664 nm, Surrelite III, Continuum). Radiation emitted from samples was first filtered through a silicon cutoff filter and subsequently wavelength-resolved with the use of a monochromator (Model M300, Edinburgh Instruments). The detection of the emitted NIR light was performed with the use of a liquid nitrogen-refrigerated NIR-sensitive photomultiplier (Model R5509, Hamamatsu Photonics) with low dark noise (<500 cps), connected to a personal computer via a 300-MHz acquisition MSA board (Becker & Hickl GmbH) (29).

Fluorescence-lifetime imaging confocal microscopy

Photosensitizer accumulation, localization, and interaction with biomolecules were observed through fluorescence-lifetime imaging confocal microscopy (FLIM). Overnight log-phase cultures of *C. albicans* (ATCC 90028) and *K. pneumoniae* (ATCC 700603) were employed. *C. albicans* was diluted in PBS to reach a working concentration at 1-2 x 10^7 CFU/mL, and *K. pneumoniae* was used at 1-2 x 10^9 CFU/mL. MB was used in a working concentration of 100 µM in PBS. Cells were not washed to remove MB from supernatant for imaging because fluorescence background (*i.e.*, outside cells) was used as intensity and lifetime controls.

Time-resolved fluorescence detection was carried out by a confocal laser scanning microscope (MicroTime 200, PicoQuant, Germany). The fluorescence system was set with 700(20) nm band-pass filters, short pulse (<1 ns) 638 nm excitation lasers, and 60x objective lens to analyze samples. Obtained images and data were analyzed by proper software (SymPhoTime 64, PicoQuant, Germany) to extract information regarding MB fluorescence lifetime.

Nanoscopy techniques - Transmission electron microscopy and atomic force microscopy coupled with infrared spectroscopy

Nanoscopy techniques were employed to visualize ultrastructural damages of treated cells. Negative controls (C-) of viable *K. pneumoniae* (ATCC 700603) cells suspended in PBS were compared to samples treated with 100 J/cm^2 of aPDT. Such a high dose was used to search for the most pronounced ultrastructural damages. Samples were fixed in 2 % glutaraldehyde kept overnight at 4° C. Then, samples were centrifuged at 10,000 g for 10 min and washed in 0.1 M sodium cacodylate buffer (pH 7.2) twice. Pellets were post-fixed in 2 % osmium tetroxide in sodium cacodylate buffer for 8 hours. Samples were then serially dehydrated in ethanol, and embedded in Spurr resin (Tousimis, USA). Ultrathin slices (<100 nm) were cut by diamond blades of an ultramicrotome (Leica, Germany).

Transmission electron microscopy (TEM) samples were placed on 200-mesh copper grids and post-stained with uranyl acetate and lead citrate solution. Sample visualization was performed on a transmission electron microscope (Model 1010, JEOL, Japan). Atomic force microscopy coupled to infrared spectroscopy (AFM-IR) samples were placed over a flat silicon crystal previously coated with 100 nm of gold by sputtering. AFM-IR sample visualization was performed by an atomic force microscope coupled with a mid-infrared quantum cascade tunable laser (NanoIR2-s, Anasys, USA) in the Laboratory of Surface Science (LCS) of the LNNano-CNPEM. The laser was set at the center of the amide I absorption band (1640 cm^{-1}). False-color scale images for AFM-IR were processed by ImageJ software (NIH, USA).

Pulsed-field gel electrophoresis - Damage of chromosomal DNA

Pulsed-field gel electrophoresis (PFGE) analysis was used to assay double-strand breaks of *K. pneumoniae* DNA. 3 control groups were employed: a negative control (C–) of viable cells suspended in PBS; a light control (CL) of cells only exposed to 100 J/cm^2; and a non-irradiated control (0) exposed only to MB at 100 µM for 60 min. aPDT experimental groups were prepared as described for inactivation studies. However, in this assay, samples were exposed to 2.5, 5, 10, 50 or 100 J/cm^2 of radiant exposure.

Following irradiation, samples were immediately transferred to Eppendorf tubes that were kept in the dark at 0-4º C. Then, samples were washed twice with cold PBS. After the third centrifugation at 6,000 g, cells were resuspended in 200 µL of TE I buffer

(Tris-HCl 10 mM, EDTA 1 mM, pH 7.5). Eighty-µL of samples were transferred into 320 µL of agarose (1 % m/v, 50-60º C) and casted into proper plug molds. Plugs were then immersed into a lysis buffer (EDTA 50 mM, Tris- HCl 50 mM, SDS 20 %, sarkosyl 1%, proteinase K 20 mg/mL, pH 7.5) for 2 h at 55º C. After lysis, plugs were washed twice in type I Milli-Q water and four times in TE I buffer at 55º C with intervals of 15 min.

For DNA cleavage, plugs were transferred into microtubes containing 10 U of Xbal restriction enzyme in TE I buffer and were incubated at 37º C for 18 h. After incubation, plugs and molecular weight standards (multimeric phase lambda DNA ladder 48, 5Kb, Bio-Rad, USA) were inserted into 1% agarose gel and immersed in TBE buffer (Tris-borate 45mM, EDTA 1 mM, pH 8,0). Electrophoresis was performed by proper equipment (Chef Mapper, Bio-Rad, USA) configured as 6 V/cm at 14º C for 22 h, with pulse intervals between 3.51 and 30.82 s. DNA was stained with ethidium bromide (1 µg/mL, Sigma-Aldrich, USA) and fluorescence images were acquired (Epi Chemi II Darkroom, UVP Bioimaging Systems, USA).

Polymerase chain reaction (PCR) assay – damage of specific genes

DNA double-strand breaks impair DNA/RNA-polymerase activity, thereby blocking gene expression and replication or amplification (30). Hence, double-strand breaks can be monitored via reduction of amplification yields of PCR reactions. Based on this principle, semi-quantitative PCR-based analysis was performed to evaluate the viability of resistance genes.

The final cell suspension was treated with aPDT under five different radiant exposures (10, 20, 30, 40 or 50 J/cm^2) or incubated with PS in the dark or treated only with light. Cells treated only with MB (0 J/cm^2) or PBS alone (C–) were used as control genes to validate the findings by comparison.

After the irradiation procedure, suspensions were washed in TBE and total nucleic acid content was extracted by boiling assay at 100º C for 15 min, in a dry block. Samples were then centrifuged at 4º C for 15 min, at 10,000 g. Total DNA was extracted from KPC-2- and IMP-1-producing *K. pneumoniae* strains (31). The amplification of the ß-lactamase encoding genes was performed according to previously established primers and conditions (32-34). PCR products were stained with GelRed (Uniscience, USA) and separated by electrophoresis in agarose gel at 1%, together with a molecular weight marker of 100 bp (New England Biolabs, USA).

Total protein and carbonyl quantification assays

Growth was performed in Mueller-Hinton broth for 20 h at 37 °C and 200 rpm. Cells were pelleted by centrifugation (6,000 g, 10 min) and washed twice with PBS. Cell density was adjusted to OD_{625nm} = 0.7 in PBS with the help of a spectrophotometer to yield 1-2 x 10^9 CFU/mL. A total of 10.8 mL of cell suspension was used for each treatment and control group.

aPDT samples were exposed to 2.5, 5, 7.5 or 10 J/cm^2 of aPDT. We also had control groups prepared without MB that were not exposed to light (C–) and that were exposed to 10 J/cm2 (CL). After irradiation, sample groups were washed twice with PBS as described previously. Each resulting cell pellet was suspended in 60 µL of sample diluent from the OxiSelect™ Protein Carbonylation Fluorimetric Assay (STA-307, Cell Biolabs Inc., USA). Cell disruption was achieved with an ultrasound cell homogenizer by pulsing cells for 5 s at 90 W of power (40 kHz, Sonifier SLPe, Soni-Tech, Brazil), followed by 5 min incubation on ice. Five cycles of pulsing-cooling were performed. Cell debris were removed by centrifugation (10,000 g, 4 °C, 5 min). A total of 50 µL were used as input and protein carbonylation analysis was performed according to the manufacturer's instructions. The assay requires protein quantification to be performed at the end of the procedure to normalize carbonyl content (nmol/mL) to protein amount (mg/mL). This quantification was carried out with Bradford Assay (Bio-Rad, USA).

ß-lactamase inhibition assay

Three control groups were used: a negative control (C–) of viable cells suspended in PBS; a light control (CL) of cells only exposed to 10 J/cm^2 without MB; and a non-irradiated control (0) exposed only to methylene blue for 60 min. aPDT experimental groups were prepared as described in the "aPDT studies for planktonic suspensions" section. For this assay, samples were exposed to 2.5, 5, 7.5 or 10 J/cm^2 of aPDT. Following irradiation, each sample was immediately transferred to an Eppendorf tube that was kept in the dark at 0-4º C. Then, the samples were washed twice with fresh PBS.

ß-lactamase activity assay (ab197008, ABCAM, UK) was performed as instructed by the manual. Briefly, pellets were weighed and suspended in the kit's assay buffer with 5 µL per milligram of the pellet. Samples were sonicated for 5 min

and centrifuged at 16,000 g at 4º C for 20 min. Two-µL of supernatant were transferred into 96-well plates containing 96 µL of assay buffer and 2 µL of nitrocefin. Plates were immediately placed in a proper spectrophotometer (SpectraMax M4, Molecular Devices, USA) and absorbance at 490 nm was measured every minute for 60 min. Measurement time-points were determined by signal saturation of C–. Absorbance data were normalized to C–.

Membrane damage assays

To verify the membrane integrity after aPDT, quantitative methods using *N*-phenyl-1-naphthylamine (NPN, Sigma-Aldrich, USA) were employed. NPN becomes fluorescent when inserted into the internal face of cell membranes and, therefore, it signalizes variations in permeability of such structures. NPN is an especially interesting probe for this study since it does not present any fluorescence excitation and emission overlaps with MB.

For these experiments, there were 4 control groups: a negative control (C–) of viable cells suspended in PBS; a positive membrane damage control (C+) of cells inactivated in 70% (v/v) propyl alcohol for 15 min; a light control (CL) of cells only exposed to 20 J/cm^2 without MB; and a non-irradiated control (0) exposed only to MB for 60 min. The aPDT experimental groups were prepared as described previously***.*** For these membrane damage assays, samples were exposed to 2.5, 5, 10 or 20 J/cm^2. Following irradiation, samples were immediately transferred to Eppendorf tubes that were kept in the dark at 0-4º C. Then, samples were washed twice with fresh PBS before they were probed with NPN.

Sample sets were distributed in 96-well plates and NPN was added to reach a final concentration of 15 µM. Plates were then kept in the dark at room temperature for 15 min. Arbitrary fluorescence intensity was measured in a proper plate reader (SpectraMax M4, Molecular Devices, USA). NPN fluorescence was excited at 350 nm and measured at 415 nm.

Statistical analysis

Experiments were performed in technical and biological triplicates for all quantitative assays. Quantitative data are presented as means and standard deviation of means. Statistical analysis for quantifications of protein content, protein carbonylation, ß-lactamase inhibition, and membrane permeability was evaluated by

multiple unpaired T-tests with comparisons to C–. Statistical differences were considered significant if $p < 0.05$. Prism 6.0 (GraphPad, USA) was used for data analysis.

Acknowledgements

We gratefully thank and technical support offered by the University of São Paulo, the Nuclear and Energy Research Institute, Brazilian Center for Research in Energy and Materials, and the start-up company BioLambda. R.O.F. thank the LNNano for providing access to the AFM-IR instrument and C. Costa (LCS) for the experimental assistance.

Funding

This work was supported by the São Paulo Research Foundation (FAPESP, grants 2019/10851-4, 2016/25095-4, 2016/25095-2, 2013/07937-8, 2017/22406-0 and 2016/08593-9) and by the National Council for Scientific and Technological Development (CNPq, grants 141901/2016-0, 465763/2014-6, 312249/2017-9, 315738/2018-9 and 433128/2018-6).

References

1. Organization WH. The evolving threat of antimicrobial resistance: Options for action [website]. WHO Publ.; 2014 [Available from: http://www.ijmr.org.in/article.asp?issn=0971-5916;year=2014;volume=139;issue=1;spage=182;epage=183;aulast=Kapi.

2. Willems RJ, Hanage WP, Bessen DE, Feil EJ. Population biology of Gram-positive pathogens: high-risk clones for dissemination of antibiotic resistance. FEMS Microbiol Rev. 2011;35(5):872-900.

3. Rice LB. Mechanisms of resistance and clinical relevance of resistance to beta-lactams, glycopeptides, and fluoroquinolones. Mayo Clin Proc. 2012;87(2):198-208.

4. Tzouvelekis LS, Markogiannakis A, Psichogiou M, Tassios PT, Daikos GL. Carbapenemases in Klebsiella pneumoniae and other Enterobacteriaceae: an evolving crisis of global dimensions. Clin Microbiol Rev. 2012;25(4):682-707.

5. Carattoli A. Plasmids and the spread of resistance. Int J Med Microbiol. 2013;303(6-7):298-304.
6. Potron A, Poirel L, Nordmann P. Emerging broad-spectrum resistance in Pseudomonas aeruginosa and Acinetobacter baumannii: Mechanisms and epidemiology. Int J Antimicrob Agents. 2015;45(6):568-85.
7. Wainwright M, Maisch T, Nonell S, Plaetzer K, Almeida A, Tegos GP, et al. Photoantimicrobials-are we afraid of the light? Lancet Infect Dis. 2017;17(2):e49-e55.
8. Hamblin MR, Hasan T. Photodynamic therapy: a new antimicrobial approach to infectious disease? Photochem Photobiol Sci. 2004;3(5):436-50.
9. Dai T, Huang YY, Hamblin MR. Photodynamic therapy for localized infections--state of the art. Photodiagnosis and photodynamic therapy. 2009;6(3-4):170-88.
10. Sabino CP, Wainwright M, Ribeiro MS, Sellera FP, Dos Anjos C, Baptista MDS, et al. Global priority multidrug-resistant pathogens do not resist photodynamic therapy. J Photochem Photobiol B. 2020;208:111893.
11. Dos Anjos C, Sellera FP, Gargano RG, Lincopan N, Pogliani FC, Ribeiro MG, et al. Algicidal effect of blue light on pathogenic Prototheca species. Photodiagnosis Photodyn Ther. 2019;26:210-3.
12. Cabral FV, Sabino CP, Dimmer JA, Sauter IP, Cortez MJ, Ribeiro MS. Preclinical Investigation of Methylene Blue-mediated Antimicrobial Photodynamic Therapy on Leishmania Parasites Using Real-Time Bioluminescence. Photochem Photobiol. 2020;96(3):604-10.
13. Baptista MS, Cadet J, Di Mascio P, Ghogare AA, Greer A, Hamblin MR, et al. Type I and Type II Photosensitized Oxidation Reactions: Guidelines and Mechanistic Pathways. Photochem Photobiol. 2017;93(4):912-9.
14. Bacellar IO, Pavani C, Sales EM, Itri R, Wainwright M, Baptista MS. Membrane damage efficiency of phenothiazinium photosensitizers. Photochemistry and photobiology. 2014;90(4):801-13.
15. Pattison DI, Rahmanto AS, Davies MJ. Photo-oxidation of proteins. Photochem Photobiol Sci. 2012;11(1):38-53.
16. Davies MJ. Singlet oxygen-mediated damage to proteins and its consequences. Biochem Biophys Res Commun. 2003;305(3):761-70.

17. Wang J, Wang S, Zhong C, Tian T, Zhou X. Novel insights into a major DNA oxidative lesion: its effects on Z-DNA stabilization. Org Biomol Chem. 2015;13(34):8996-9.
18. Nogueira JJ, Gonzalez L. Molecular dynamics simulations of binding modes between methylene blue and DNA with alternating GC and AT sequences. Biochemistry. 2014;53(14):2391-412.
19. Agnez-Lima LF, Melo JT, Silva AE, Oliveira AH, Timoteo AR, Lima-Bessa KM, et al. DNA damage by singlet oxygen and cellular protective mechanisms. Mutat Res. 2012.
20. Singh TA, Rao BS, O'Neill P. Radical chemistry of 8-oxo-7,8-dihydro-2'-deoxyadenosine and 8-oxo-7,8-dihydro-2'-deoxyguanosine: a pulse radiolysis study. J Phys Chem B. 2010;114(49):16611-7.
21. Davies MJ. Protein oxidation and peroxidation. Biochem J. 2016;473(7):805-25.
22. Daly MJ. Death by protein damage in irradiated cells. DNA Repair (Amst). 2012;11(1):12-21.
23. Krisko A, Radman M. Protein damage and death by radiation in Escherichia coli and Deinococcus radiodurans. Proc Natl Acad Sci U S A. 2010;107(32):14373-7.
24. Qi HZ, Wang WZ, He JY, Ma Y, Xiao FZ, He SY. Antioxidative system of Deinococcus radiodurans. Res Microbiol. 2020;171(2):45-54.
25. Nitzan Y, Ashkenazi H. Photoinactivation of Deinococcus radiodurans: An Unusual Gram-Positive Microorganism. Photochemistry and Photobiology. 2008;69(4):5.
26. Brancini GT, Rodrigues GB, Rambaldi MS, Izumi C, Yatsuda AP, Wainwright M, et al. The effects of photodynamic treatment with new methylene blue N on the Candida albicans proteome. Photochem Photobiol Sci. 2016;15(12):1503-13.
27. Sabino CP, Wainwright M, Dos Anjos C, Sellera FP, Baptista MS, Lincopan N, et al. Inactivation Kinetics and Lethal Dose Analysis of Antimicrobial Blue Light and Photodynamic Therapy. Photodiagnosis Photodyn Ther. 2019.
28. Jett BD, Hatter KL, Huycke MM, Gilmore MS. Simplified agar plate method for quantifying viable bacteria. Biotechniques. 1997;23(4):648-50.
29. Oliveira CS, Turchiello R, Kowaltowski AJ, Indig GL, Baptista MS. Major determinants of photoinduced cell death: Subcellular localization versus photosensitization efficiency. Free radical biology & medicine. 2011;51(4):824-33.

30. Laval J. Role of DNA repair enzymes in the cellular resistance to oxidative stress. Pathol Biol (Paris). 1996;44(1):14-24.
31. Chapman PA, Ellin M, Ashton R, Shafique W. Comparison of culture, PCR and immunoassays for detecting Escherichia coli O157 following enrichment culture and immunomagnetic separation performed on naturally contaminated raw meat products. Int J Food Microbiol. 2001;68(1-2):11-20.
32. Woodford N. Rapid characterization of beta-lactamases by multiplex PCR. Methods Mol Biol. 2010;642:181-92.
33. Lincopan N, McCulloch JA, Reinert C, Cassettari VC, Gales AC, Mamizuka EM. First isolation of metallo-beta-lactamase-producing multiresistant Klebsiella pneumoniae from a patient in Brazil. J Clin Microbiol. 2005;43(1):516-9.
34. Oliveira S, Moura RA, Silva KC, Pavez M, McCulloch JA, Dropa M, et al. Isolation of KPC-2-producing Klebsiella pneumoniae strains belonging to the high-risk multiresistant clonal complex 11 (ST437 and ST340) in urban rivers. J Antimicrob Chemother. 2014;69(3):849-52.